Ocean Modelling 42 (2012) 50–56

Contents lists available at SciVerse ScienceDirect

Ocean Modelling

journal homepage: www.elsevier.com/locate/ocemod

Large near-inertial oscillations of the Atlantic meridional overturning circulation ☆

Adam T. Blaker [a,*], Joël J-M. Hirschi [a], Bablu Sinha [a], Beverly de Cuevas [a], Steven Alderson [a], Andrew Coward [a], Gurvan Madec [a,b]

[a] National Oceanography Centre, Southampton, Southampton, SO14 3ZH, UK
[b] LOCEAN (CNRS/IRD/UPMC/MNHN) Institut Pierre et Simon Laplace, Paris, France

ARTICLE INFO

Article history:
Received 17 August 2011
Received in revised form 15 November 2011
Accepted 18 November 2011
Available online 6 December 2011

Keywords:
Meridional overturning circulation
High frequency variability
Near inertial gravity waves
Ocean model

ABSTRACT

The Atlantic meridional overturning circulation (AMOC) is a key contributor to Europe's mild climate. Both observations and models suggest that the AMOC strength varies on a wide range of timescales. Here we show the existence of previously unreported large near inertial AMOC oscillations in a high resolution ocean model. Peak-to-peak these oscillations can exceed 50 Sv ($50 \cdot 10^6\ m^3\ s^{-1}$) in one day. The AMOC oscillations are caused by equatorward propagating near-inertial gravity waves (NIGWs) which are forced by temporally changing wind forcing. The existence of NIGWs in the ocean is supported by observations, and a significant fraction of the ocean's kinetic energy is associated with the near inertial frequencies. Our results also suggest that the NIGW-driven MOC variability would be near invisible to contemporary AMOC observing systems such as the RAPID MOC system at 26.5°N.

1. Introduction

The Atlantic meridional overturning circulation (AMOC) is part of the global ocean conveyor which transports warm and saline surface waters to the North Atlantic (Broeker, 1987; Dickson and Brown, 1994; Kuhlbrodt et al., 2007). On their journey towards the Nordic seas these surface waters gradually become denser as they release heat to the atmosphere. Eventually, the increasing density leads to the sinking of the water masses and they are returned southward as cold and dense North Atlantic deep water. In the subtropical North Atlantic the surface and deep branches of the AMOC result in a maximum net northward heat transport of more than 1 PW (Ganachaud and Wunsch, 2000; Lumpkin and Speer, 2007; Johns et al., 2011). The AMOC has been identified as a key ocean mechanism which contributes to the comparatively mild European climate. A large fraction of the heat released to the atmosphere by the AMOC is carried eastward towards Europe by the predominant westerly winds, leading to warmer temperatures in northwestern Europe than at similar latitudes in western Canada (Rhines and Häkkinen, 2003; Broeker, 1987).

Paleoclimate records suggest that in the past the AMOC is likely to have undergone major rapid fluctuations (McManus et al., 2004). Furthermore, most climate models suggest that under anthropogenic greenhouse gas forcing the AMOC will likely undergo a 30% reduction by the year 2100 (IPCC, 2007; Gregory et al., 2005). Any change in the strength of the AMOC would affect the northward transport of heat and therefore the climate over the North Atlantic region. Additionally, a change in the strength of the AMOC may also impact the capacity of the North Atlantic to absorb greenhouse gases.

Recent observation-based studies have shown the AMOC transport at 26.5°N to exhibit substantial variability on short timescales (Cunningham et al., 2007; Kanzow et al., 2009; Kanzow et al., 2010). Between April 2004 and April 2009, the maximum AMOC transport at 26.5°N has a mean of 18.54 Sv, with a standard deviation of 4.68 Sv. The intra-annual peak-to-peak range of the AMOC can be as large as 30 Sv (Cunningham et al., 2007). The origin of the observed large AMOC variability is only partly understood. Some variability, such as the observed seasonality of the AMOC, can be linked to the seasonal variability in the wind stress curl along the African coast (Kanzow et al., 2010). The contribution to the observed AMOC variability by mechanisms such as baroclinic Kelvin waves (Kawase, 1987; Johnson and Marshall, 2002) or Rossby waves (Hirschi et al., 2007) has yet to be established. However, the existence of large AMOC variability on short timescales has been confirmed in both observations (Cunningham et al., 2007; Kanzow et al., 2009; Kanzow et al., 2010) and numerical ocean and coupled-climate models (Hirschi and Marotzke, 2007; Baehr et al., 2007; Baehr et al., 2009; Balan Sarojini et al., 2011).

To better understand the AMOC variability on short timescales we use a global ocean/sea-ice model with a nominal grid resolution of 0.25°, sufficient to resolve western boundary current structures and to simulate the main processes associated with deep water formation necessary to model the AMOC. Two model integrations

☆ National Oceanography Centre, Southampton, University of Southampton Waterfront Campus, European Way, Southampton, SO14 3ZH, UK.
* Corresponding author. Tel.: +44 (0)2380 596 312.
E-mail address: atb299@noc.ac.uk (A.T. Blaker).

1463-5003/$ - see front matter Crown Copyright © 2011 Published by Elsevier Ltd. All rights reserved.
doi:10.1016/j.ocemod.2011.11.008

where model output is stored at high frequency reveal some interesting large amplitude variability in the AMOC.

2. Description of the model and numerical integrations

We use NEMO v3.0 (Nucleus for European Modelling of the Ocean) (Madec, 2008) in the Global ORCA025 configuration set up in the DRAKKAR project (DRAKKAR Group, 2007; Barnier et al., 2006; Madec, 2008). Horizontal resolution is 1/4° (1442 × 1021 grid points). South of 20°N the model grid is isotropic Mercator, and north of 20°N the grid becomes quasi-isotropic bipolar, with poles located in Canada and Siberia to avoid the numerical instability associated with the convergence of the meridians at the geographic north pole. At the Equator the resolution is approximately 27.75 km, becoming finer at higher latitudes such that at 60°N/S it becomes 13.8 km. The model has 64 vertical levels with a grid spacing increasing from 6 m near the surface to 250 m at 5500 m. Bottom topography is represented as partial steps and bathymetry is derived from ETOPO2 (U.S. Department of Commerce, 2006). To prevent excessive drifts in global salinity due to deficiencies in the fresh water forcing, sea surface salinity is relaxed towards climatology with a piston velocity of 33.33 mm/day/psu. Sea ice is represented by the Louvain-la-Neuve Ice Model version 2 (LIM2) sea-ice model (Timmerman et al., 2005).

Starting from rest the model simulates the period 1958–2001, with surface forcing comprising of 6-hourly mean momentum fields, daily mean radiation fields and monthly mean precipitation fields supplied by the DFS4.1 dataset (Brodeau et al., 2010) and linearly interpolated from the time mean fields by the model. Model output is stored as 5-day averages. Starting from the ocean state on January 1st 1989 in the simulation described above, we perform two additional NEMO ORCA025 integrations where a 2-month period (January 1st 1989 to February 28th 1989) is re-run and where model output is stored as 4-hourly averages. The first integration uses the same surface forcing as before. In the second integration the wind forcing is held temporally constant by applying the wind forcing on the first model timestep to all subsequent integration timesteps.

3. Analysis and decomposition of the AMOC

We calculate the AMOC, $\Psi_{mod}(y,z)$, as the zonal and vertical integral of $v\,(x,y,z)$, the meridional velocity, i.e.

$$\Psi_{mod}(y,z) = \int_{-H_{max}(y)}^{z} \int_{x_w}^{x_e} v(x,y,z')\,dxdz', \tag{1}$$

where x_w and x_e are the western and eastern boundaries of the ocean basin respectively, $-H_{max}(y)$ is the maximum depth of the ocean basin and z is the vertical coordinate.

The time mean AMOC in NEMO (Fig. 1) compares well with other models. Typical of most ocean models, the return flow in the deep ocean is too shallow, by a few hundred metres, but the depth of the maximum value, at 1000 m, compares well with observations (Kanzow et al., 2009). At 26.5°N and 1000 m depth the AMOC calculated from a typical 5 year period, equivalent to the current length of the RAPID 26.5°N observations, is 22.54 Sv, 4 Sv higher than RAPID observations, and the standard deviation is 4.1 Sv, ~10% lower than observed.

3.1. Decomposition of the AMOC

The model AMOC, Ψ_{mod}, can be decomposed into one barotropic and three baroclinic component parts, each representing a different physical process and corresponding to the components which are measured by the RAPID observing array (Hirschi and Marotzke, 2007),

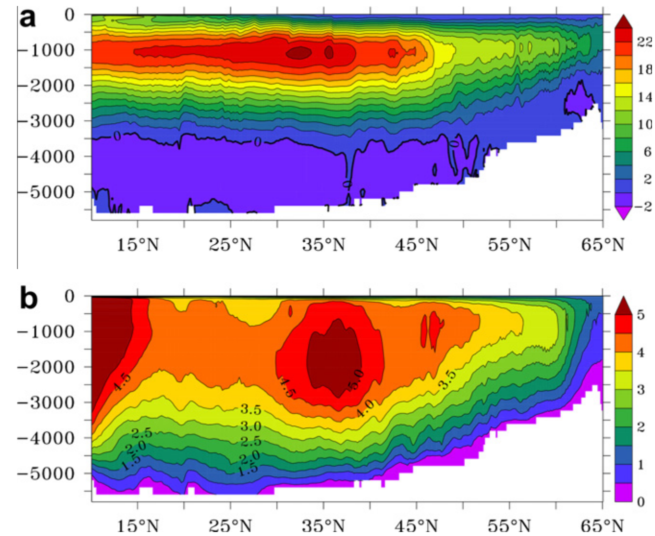

Fig. 1. Latitude-depth plots of the AMOC (Sv) for the period 1989–1995: (**a**), time mean and (**b**), standard deviation based on 5 day mean model output.

$$\Psi_{mod} = \Psi_{btr} + \Psi_{geo} + \Psi_{ekm} + \Psi_{res} \tag{2}$$

Ψ_{btr} is the barotropic component arising from depth averaged velocities,

$$\Psi_{btr}(y,z) = \int_{-H_{max}(y)}^{z} \int_{x_w}^{x_e} \bar{v}(x,y)\,dxdz' \tag{3}$$

in which

$$\bar{v}(x,y) = \frac{1}{H(x,y)} \int_{-H(x,y)}^{0} v(x,y,z')\,dz' \tag{4}$$

is the barotropic meridional velocity. $\Psi_{geo}(y,z)$, the baroclinic geostrophic (or thermal wind) component arising from zonal density gradients across the Atlantic basin is

$$\Psi_{geo}(y,z) = \int_{-H_{max}(y)}^{z} \int_{x_w}^{x_e} (v_{geo}(x,y,z') - \bar{v}_{geo}(x,y))\,dxdz', \tag{5}$$

where v_{geo} and $\bar{v}_{geo}$ are

$$v_{geo}(x,y,z) = -\frac{g}{\rho^* f} \int_{-H(x,y)}^{z} \frac{\partial \rho}{\partial x}\,dz' \tag{6}$$

and

$$\bar{v}_{geo}(x,y) = \frac{1}{H(x,y)} \int_{-H(x,y)}^{0} v_{geo}(x,z')\,dz' \tag{7}$$

respectively, g being the Earth's gravitational acceleration, ρ the in situ density, f the Coriolis parameter, and ρ^* a reference density. $\Psi_{ekm}(y,z)$, the Ekman (wind driven) component compensated by a section mean return flow to ensure no net transport is,

$$\Psi_{ekm}(y,z) = \int_{-H_{max}(y)}^{z} \int_{x_w}^{x_e} (v_{ekm}(x,y,z') - \bar{v}_{ekm}(x,y))\,dxdz', \tag{8}$$

where $v_{ekm}(x,y,z')$ and $\bar{v}_{ekm}(x,y)$ are

$$v_{ekm}(x,y,z) = -\frac{1}{(\rho^* f L \Delta_z)} \int_{x_w}^{x_e} \tau_x\,dx \tag{9}$$

and

$$\bar{v}_{ekm}(x,y) = -\frac{1}{(\rho^* f A)} \int_{x_w}^{x_e} \tau_x dx \tag{10}$$

respectively, L being the basin width, Δ_z the Ekman depth, and A the cross-sectional area of the basin. The Ekman depth, Δ_z, which